Peer-reviewed version available at Crystals 2017, 7, 379; doi:10.3390/cryst7120379

Article

Influence of Alkali Metal Substitution on the Phase Transition Behavior of $CsGaQ_2$ (Q = S, Se)

Daniel Friedrich [1], Marc Schlosser [1], Martin Etter [2] and Arno Pfitzner [1,*]

[1] Institut für Anorganische Chemie, Universität Regensburg, Universitätsstraße 31, 93040 Regensburg, Germany
[2] Deutsches Elektronensynchrotron (DESY), Notkestraße 85, 22607 Hamburg, Germany
* Correspondence: arno.pfitzner@chemie.uni-regensburg.de; Tel.: +49-941-943-4551

Abstract: The formation of solid solution series $Cs_{1-x}M_xGaQ_2$-$mC64$ (M = K, Rb; Q = S, Se; x = 0–1) was studied by X-ray diffraction and spectroscopic methods, revealing a complete miscibility of $CsGaQ_2$-$mC64$ with $RbGaQ_2$ and $KGaSe_2$, and a large miscibility gap with $KGaS_2$. All solid solution members exhibit similar Raman spectra, indicating the covalent Ga-Q bonding character. The similar optical band gaps likewise further contribute to this conclusion. Up to a degree of substitution, these solid solutions undergo a phase transition similar to $CsGaQ_2$-$mC64$. The influence of the substitution parameter x on phase transition process was investigated *in situ* using high-temperature X-ray powder diffraction experiments. Phase-pure solid solutions of the high-temperature polymorphs $Cs_{1-x}M_xGaQ_2$-$mC16$ were obtained up to x_{max}(K) = 0.1 and x_{max}(Rb) = 0.3. The crystal structures of these new $CsGaQ_2$-$mC16$ analogous high-temperature phases were refined from synchrotron diffraction data by Rietveld-refinement.

Keywords: chalcogenogallates; polymorphism; solid solutions; *in situ* X-ray diffraction; synchrotron radiation; rietveld refinement

---

1. Introduction

Chalcogenometallates of the group 13 metals containing alkali metal cations $M_xT_yQ_z$ (M = alkali metal, T = triel, Q = chalcogen) are interesting materials for technical applications because of their semiconducting properties [1]. These solids crystallize in a large variety of different crystal structures [2]. The main structural features of these compounds are the oligomeric or polymeric one-, two- or three-dimensional (1D, 2D, 3D) anions formed by condensed TQ_4 tetrahedra. The crystal structures of the resulting solids contain these anionic chains, layers or networks embedded in a surrounding of the alkali metal cations. Among all known compounds, the MTQ_2 phases are known for most of the possible element combinations. The dominating structure type among these solids is the $TlGaSe_2$ structure type [3], featuring anionic layers $^2_\infty[T_4Q_8^{4-}]$. This structure type obviously has a very high tolerance for different combinations of the involved elements. Another structural motif of MTQ_2 phases are the anionic chains $^1_\infty[TQ_2^-]$ found in the Tl_2Se_2 [4] and $KFeS_2$ [5] structure types, respectively. Only the high-temperature polymorphs of $CsGaS_2$ [6] and $CsGaSe_2$ [7] crystallize in the latter type, but no analogous phase transition is known for the lighter homologous compounds. This behavior likely results from the higher degree of spatial separation necessary for the formation of one-dimensional structures which can only be realized by the larger cesium cations.

Herein, we report on the synthesis of new phases with $KFeS_2$ structure type. Based on our investigations on the high-temperature phase transitions of $CsGaS_2$ and $CsGaSe_2$, we decided to explore the possibilities of the formation of solid solutions of these compounds with $RbGaQ_2$ and $KGaQ_2$. As the compounds $KGaQ_2$ [8-9], $RbGaQ_2$ [10-11] and the low-temperature phases $CsGaQ_2$-$mC64$ [6-7] (Q = S, Se) all crystallize isotypic in the $TlGaSe_2$ structure type, the formation of solid solutions $Cs_{1-x}M_xGaQ_2$-$mC64$ (M = K, Rb; Q = S, Se; x = 0 - 1) should be possible. $CsGaTe_2$ [12] also crystallizes in the $TlGaSe_2$ structure type, but no phase transition occurs upon heating of this

Preprints (www.preprints.org) | NOT PEER-REVIEWED | Posted: 20 October 2017 doi:10.20944/preprints201710.0140.v1

Peer-reviewed version available at *Crystals* **2017**, *7*, 379; doi:10.3390/cryst7120379

compound. Therefore, no solid solutions using this phase were attempted. The influence of the alkali metal substitution on the high-temperature phase transition behavior of the cesium compounds was further studied *in situ* by using high-temperature X-ray diffraction techniques. Using this substitution approach, the isolation of new $KFeS_2$ type phases $Cs_{1-x}M_xGaQ_2$-*mC*16 is possible. The solid solutions were also studied by Raman spectroscopy. Furthermore, the influence of the alkali metal substitution on the band gaps of these semiconductors was investigated by UV/Vis diffuse reflectance spectroscopy. The crystal structures of the new high-temperature phases were refined from synchrotron powder diffraction data by Rietveld refinement.

2. Results

2.1. Crystal structures of the CsGaQ₂ polymorphs

As all investigated compounds and solid solutions in this paper are related to the polymorphic modifications of $CsGaS_2$ and $CsGaSe_2$, the crystal structures of these polymorphs will be discussed beforehand. The low-temperature polymorph $CsGaQ_2$-*mC*64 [6-7], as well as $KGaQ_2$ [8-9] and $RbGaQ_2$ (Q = S, Se) [10-11], crystallize in the $TlGaSe_2$ structure type (Figure 1). The $TlGaSe_2$ structure type features anionic 2D layers $^2_\infty[Ga_4Q_8{}^{4-}]$, composed of vertex-sharing Ga_4Q_{10} supertetrahedra, stacked along [001]. These layers are penetrated by cesium cations. The cesium cations are 6+2 fold coordinated by chalcogen atoms, resulting in bicapped trigonal prisms.

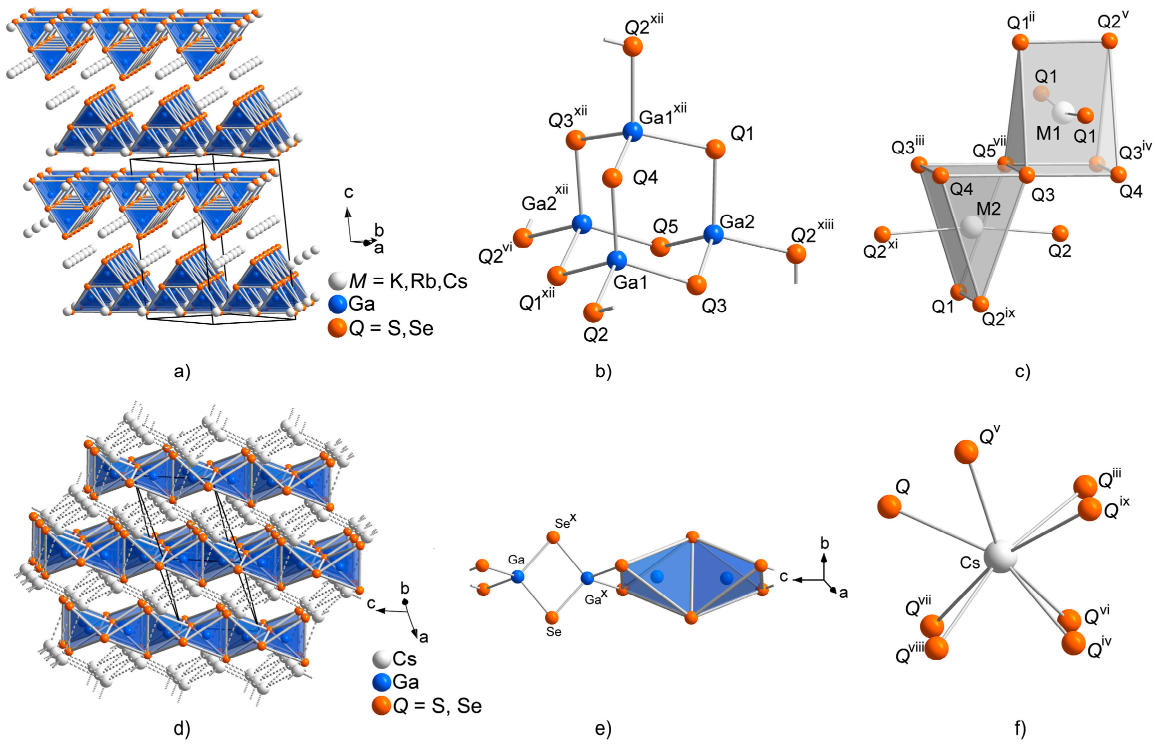

Figure 1. Comparison of the crystal structures of the $TlGaSe_2$ (a-c) and the $KFeS_2$ (d-f) structure types, showing: a) the stacking of the anionic layers in the $TlGaSe_2$ structure type; b) the supertetrahedral building blocks Ga_4Q_{10} of these layers; c) coordination polyhedra of the alkali metal sites; d) the arrangement of the anionic chains in the $KFeS_2$ structure type; e) the SiS_2 analogous anionic chain; f) the coordination of the cesium site.

The high-temperature polymorphs $CsGaQ_2$-*mC*16 (Q = S, Se) crystallize in the $KFeS_2$ structure type (Figure 1). This structure type features 1D, anionic chains $^1_\infty[GaQ_2{}^-]$ along [001], formed by edge-sharing tetrahedra. These chains form a hexagonal rod packing embedded in a cationic network with a topology similar to cubic diamond. The cesium cations are eightfold coordinated by the chalcogenide anions, resulting in an irregular polyhedron. Contrary to the low-temperature phase,

Preprints (www.preprints.org) | NOT PEER-REVIEWED | Posted: 20 October 2017 doi:10.20944/preprints201710.0140.v1

Peer-reviewed version available at *Crystals* **2017**, *7*, 379; doi:10.3390/cryst7120379

which obviously has a very high tolerance for different combinations of the involved elements, only cesium compounds crystallize in this structure type. This is likely due to the higher degree of spatial separation necessary for the formation of the 1D structure which can only be realized by the larger cesium cations.

2.2. Formation of solid solutions $Cs_{1-x}M_xGaQ_2$-mC64 (M = K, Rb; Q = S, Se; x = 0 - 1)

In order to prepare the solid solution series $Cs_{1-x}M_xGaQ_2$-*mC*64 (*M* = K, Rb; *Q* = S, Se; *x* = 0 - 1) the ternary phases $CsGaQ_2$-*mC*64 were mixed with stoichiometric amounts of $RbGaQ_2$ or $KGaQ_2$. *x* was varied in steps of 0.1, *i. e.* 10 %, for all series under discussion. These mixtures were thoroughly ground in an agate mortar and pressed to compact pellets. The pellets were annealed at 550 °C (slightly below the phase transition temperature of pure $CsGaQ_2$-*mC*64 [6-7]) for 7 days. This step was repeated two more times in order to ensure a maximum intermixture of the starting phases. Afterwards, the samples were homogenized again and investigated by X-ray powder diffraction.

2.2.1. X-ray diffraction experiments

The various diffraction patterns of all solid solution members are shown in the Figures S1-S4. All diffraction patterns resemble the ternary end members, indicating the formation of solid solutions. Accordingly, all reflections shift towards larger 2θ values with decreasing cesium content. For the samples with a composition $Cs_{1-x}K_xGaS_2$-*mC*64 (*x* = 0.4 – 0.7), a significant broadening of the reflections and additional reflections originating from Ga_2S_3 were observed. This indicates an incomplete mixture of $KGaS_2$ and $CsGaS_2$-*mC*64. Figure 2 shows a plot of the refined cell volumes *vs.* the composition of the different samples.

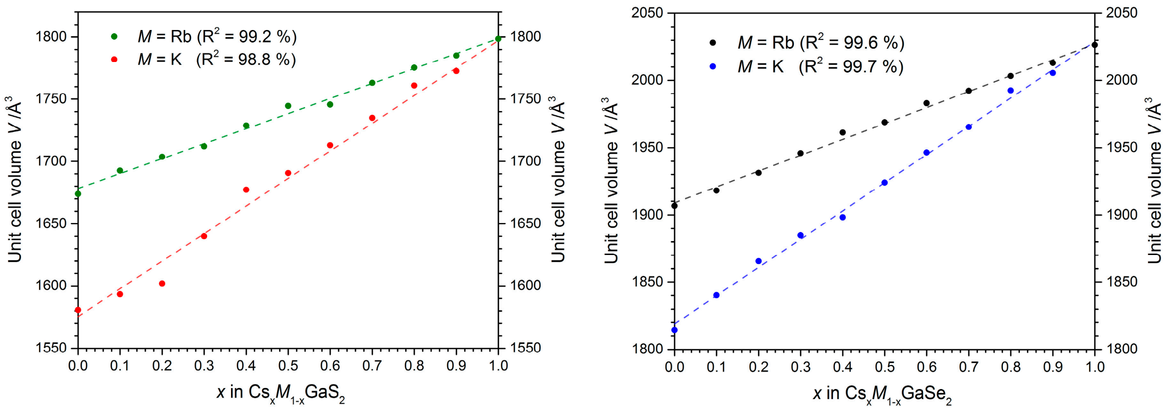

Figure 2. Plots of the unit cell volumes *vs.* the composition of the solid solutions $Cs_{1-x}M_xGaS_2$-*mC*64 (*M* = K, Rb; *x* = 0 - 1) and $Cs_{1-x}M_xGaSe_2$-*mC*64 (*M* = K, Rb; *x* = 0 - 1). The dashed lines indicate a linear fit. E.s.d.s are within the size of the spots.

An increasing unit cell volume with increasing cesium content is observed in all four cases as a general trend. However, a significant deviation from an ideal linear dependence is observed in case of the sulfide samples. This scattering is most pronounced in the series $Cs_{1-x}K_xGaS_2$.

2.2.2. Raman spectroscopy

As all end members and solid solutions under discussion crystallize in the same crystal structure type, we could study the influence of the alkali metal substructure on the vibrational frequencies of these chalcogenotrielates. The Raman spectra of the pure phases $KGaQ_2$, $RbGaQ_2$ and $CsGaQ_2$-*mC*64, as well as the spectra of the solid solutions $Cs_{1-x}M_xGaQ_2$-*mC*64 (*M* = K, Rb; *Q* = S, Se; *x* = 0 - 1) are shown in Figure 3. The Raman spectra of the ternary phases $KGaQ_2$, $RbGaQ_2$ and $CsGaQ_2$-*mC*64 revealed an almost identical pattern for the sulfides and selenides, respectively.

Preprints (www.preprints.org) | NOT PEER-REVIEWED | Posted: 20 October 2017 doi:10.20944/preprints201710.0140.v1

Peer-reviewed version available at Crystals 2017, 7, 379; doi:10.3390/cryst7120379

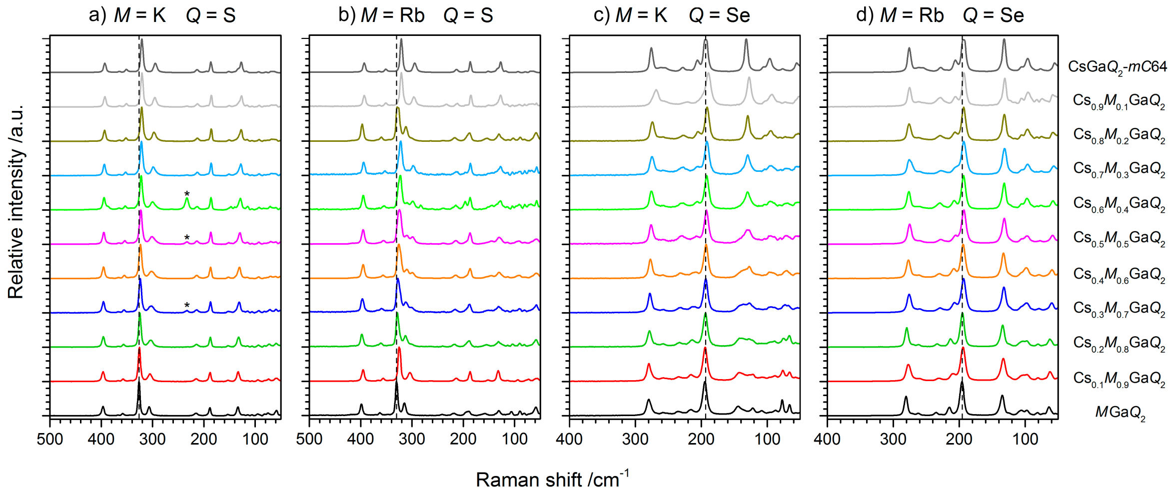

Figure 3. Raman spectra of the solid solution series $Cs_{1-x}M_xGaQ_2$-*mC*64 a) $Cs_{1-x}K_xGaS_2$-*mC*64, b) $Cs_{1-x}Rb_xGaS_2$-*mC*64, c) $Cs_{1-x}K_xGaSe_2$-*mC*64, and d) $Cs_{1-x}Rb_xGaSe_2$-*mC*64. As a reference, the position of the strongest vibration of the pure cesium phases is highlighted by a dashed line.

Consequently, the Raman spectra of all members of the solid solution series $Cs_{1-x}M_xGaQ_2$-*mC*64 (*M* = K, Rb; *Q* = S, Se; *x* = 0 - 1) also show an identical pattern. This observation confirms that only Ga-*Q* vibrations of the anionic substructure appear in the Raman spectra of these compounds, at least in the detected frequency range. The slight blue shift of all vibrations in the spectra of the lighter alkali metals indicate slightly stronger bonds Ga-*Q*, corresponding to the smaller distances *d*(Ga-*Q*) in the rubidium and potassium compounds. In the solid solutions $Cs_{1-x}Rb_xGaS_2$-*mC*64 (*x* = 0.3 – 0.6), we could observe one weak peak at 240 cm^{-1} which can be attributed to the strongest vibration of *α*-Ga_2S_3. As this impurity phase is not visible in the X-ray patterns of any of the ternary phases used for the synthesis, this observation could be another hint for an incomplete solid solution of the sulfides at ambient conditions. Other hints for incomplete mixtures like peak broadening or splitting, however, could not be observed in the Raman spectra.

2.2.3. Optical properties

The influence of the alkali metal substitution on the electronic structure, especially the optical band gaps of the solid solutions, was investigated by UV/Vis diffuse reflectance spectroscopy. As only the optical band gaps of $KGaSe_2$, $CsGaSe_2$-*mC*64 and $CsGaS_2$-*mC*64 are reported in literature, we measured the missing band gaps for a complete study (Figure 4).

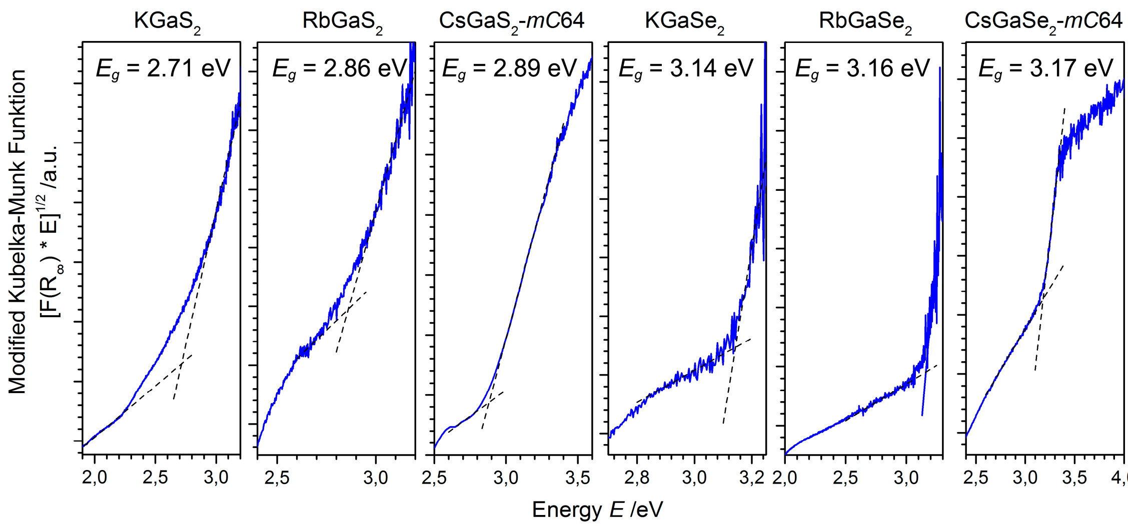

Preprints (www.preprints.org) | NOT PEER-REVIEWED | Posted: 20 October 2017 doi:10.20944/preprints201710.0140.v1

Peer-reviewed version available at Crystals 2017, 7, 379; doi:10.3390/cryst7120379

Figure 4. Diffuse reflectance spectra of $MGaQ_2$ (M = K, Rb, Cs; Q = S, Se) compounds. The data for $CsGaQ_2$-*mC*64 and $RbGaSe_2$ was taken from the respective literature [6-7, 11].

The comparison of all spectra reveals almost identical band gaps for the respective sulfide and selenium compounds. This observation can easily be interpreted by DFT simulations performed by Feng *et al.* for $KGaSe_2$ [8] and by us for the cesium compounds [6-7, 13] and $RbGaSe_2$ [11]. While these calculated values are in good agreement with experimental data for the sulfides, significant deviations (> 1 eV) between the experimental and calculated band gaps were obtained for all selenides.[7-11] The smaller calculated band gaps in case of the selenides indicate that conventional calculations apparently underestimate the Ga-Se interactions between the selenogallate layers. For all compounds, however, a similar bonding situation was derived from these calculations. The bonding character of the alkali metals in these compounds is mainly ionic, which can be concluded from the unoccupied K-4*s*, Rb-5*s* and Cs-6*s* states, respectively. Ga-*Q* interactions within the GaQ_4 tetrahedra cause a splitting into valence- and conduction band. The band gaps are mostly dominated by the Ga-4*s*, Ga-4*p* and the respective *p* states of the chalcogen atoms (S-3*p* or Se-4*p*). The highest occupied alkali metal states (K-3*p*, Rb-4*p* or Cs-5*p*) are located at energies below -10 eV, and therefore do not contribute to the states near the band gap, resulting in similar experimental values.

2.3. High-temperature phase transition

2.3.1. Influence of the alkali metal substitution on the phase transition behavior

Following the successful preparation of the solid solution series $Cs_{1-x}M_xGaQ_2$-*mC*64 (M = K, Rb; Q = S, Se; x = 0 - 1) we decided to study the influence of the alkali metal substitution on the high-temperature behavior (especially the phase transition) of these compounds. An initial analysis using differential thermal analysis (DTA) was not successful, as in most cases, no thermal effect could be detected. An investigation of the resulting samples using X-ray powder diffraction, however, revealed that in some cases the phase transition proceeded nevertheless. Therefore, we investigated these substances *in situ* using high-temperature X-ray powder diffraction techniques. All experiments were performed with the same experimental conditions (grain-size, temperature program etc.) to ensure a good comparability of the data. The experiments were performed in the temperature range from 20 – 900 °C. In case of a complete phase transition below 900 °C, the experiment was aborted below the maximum temperature. In order to check for a possible phase transition of $KGaQ_2$ and $RbGaQ_2$, these compounds were also investigated by *in situ* powder diffraction at elevated temperatures.

The *in situ* experiments revealed a similar behavior of all four solid solution series at elevated temperatures (Supplement Figure S5). For the pure cesium phases a phase transition occurs at 600 °C for $CsGaS_2$-*mC*64 and 620 °C for $CsGaSe_2$-*mC*64, respectively. An increase of the potassium or rubidium content in these phases has an influence on the starting temperature and the time necessary for this phase transition. With a decreasing cesium content, the start of the phase transition shifts to higher temperatures. For the solid solutions $Cs_{1-x}K_xGaS_2$-*mC*64 ($0 \leq x \leq 0.6$), $Cs_{1-x}Rb_xGaS_2$-*mC*64 ($0 \leq x \leq 0.6$), $Cs_{1-x}K_xGaSe_2$-*mC*64 ($0 \leq x \leq 0.4$), and $Cs_{1-x}Rb_xGaSe_2$-*mC*64 ($0 \leq x \leq 0.6$), a phase transition to the *mC*16 type structure is observed. The selenides with potassium content higher than 40 %, however, melt before this solid-solid phase transition occurs. Samples with a higher degree of substitution do not show the *mC*64 to *mC*16 phase transition at all.

In order to test which solid solution members actually produced pure samples of the high-temperature phases $Cs_{1-x}M_xGaQ_2$-*mC*16 (M = K, Rb; Q = S, Se; x = 0 - 1), each sample of the solid solutions $Cs_{1-x}M_xGaQ_2$-*mC*64 (M = K, Rb; Q = S, Se; x = 0 – 1) was annealed at 950 °C for one week, quenched in ice water, and investigated by X-ray diffraction. This treatment should answer the question, whether the phase transition progressed until completion, or a phase separation takes place at high temperature. Among all samples, only $Cs_{0.9}K_{0.1}GaQ_2$, $Cs_{0.8}K_{0.2}GaS_2$, $Cs_{0.9}Rb_{0.1}GaQ_2$,

Peer-reviewed version available at Crystals 2017, 7, 379; doi:10.3390/cryst7120379

$Cs_{0.8}Rb_{0.2}GaQ_2$, and $Cs_{0.7}Rb_{0.3}GaQ_2$ (Q = S, Se) showed a phase pure X-ray diffraction pattern analogous to the $KFeS_2$ structure type. Up to a composition of $Cs_{0.6}K_{0.4}GaS_2$, $Cs_{0.5}K_{0.5}GaSe_2$, $Cs_{0.5}Rb_{0.5}GaS_2$, and $Cs_{0.5}Rb_{0.5}GaSe_2$, a separation into a mixture of a $TlGaSe_2$ and a $KFeS_2$ analogous phase could be detected. This mixture is likely composed of a cesium rich solid solution, which underwent a phase transition to the high-temperature polymorph and a corresponding rubidium/potassium rich phase which does not transform. A higher degree of substitution does not lead to a phase transition at all, which is in good agreement with the results of the *in situ* measurements.

2.1.1. Structure refinement of new $Cs_{1-x}M_xGaQ_2$-*mC*16 (M = K, Rb; Q = S, Se) phases

In order to analyze the crystal structures of these $CsGaQ_2$-*mC*16 (Q = S, Se) analogous solid solutions, we decided to perform Rietveld refinements of the phase pure high-temperature polymorphs. Most diffraction patterns had a bad signal to noise ratio due to the relatively high absorption coefficient (cesium) and X-ray fluorescence (rubidium, selenium) when using Mo-radiation. We therefore collected high quality synchrotron diffraction data using a custom wavelength of λ = 0.20717 Å at the P02.1 beamline at PETRA III (DESY, Hamburg). These measurements revealed that the mixtures $Cs_{0.7}Rb_{0.3}GaSe_2$, $Cs_{0.8}K_{0.2}GaS_2$, and $Cs_{0.9}K_{0.1}GaSe_2$ also contained traces of the low-temperature polymorphs which were not detected from the in-house measurements using Mo-radiation. After indexing of the observed reflections of all samples, we obtained slightly smaller cell volumes compared to the pure cesium compounds $CsGaS_2$-*mC*16 (V = 493.8(1) Å^3) and $CsGaSe_2$-*mC*16 (V = 544.3(3) Å^3), as well as some deviations in the reflection intensities. This indicates that another alkali metal was indeed incorporated into the crystal structures. As a starting model for the Rietveld refinement, we used the solution obtained from charge flipping methods using SUPERFLIP [14] (implemented in Jana2006 [15]). After splitting of the alkali metal site for Cs and M (M = K, Rb) and linking the occupation factors of both alkali metals to ensure charge balance, we tested several different models (1-3) for the structure refinement.

(1) Using the least possible number of restrictions, we initially refined all atomic coordinates and displacement parameters independently with only the occupation factors of the alkali metals restrained to sum up to 1. While this procedure worked for all structures, reasonable refinements could only be obtained using isotropic displacement parameters. Furthermore, some refinements converged with unreasonable large or small displacement parameters of the minority alkali metal. (2) The best structural R values were obtained by separate refinement of the displacement parameters and atomic coordinates of two independent alkali metal positions. Due to the high cesium content in all solid solutions, only the Cs site could be refined with anisotropic displacement parameters, while isotropic displacement parameters were applied for Rb and K sites, respectively. Even though these refinements yielded the best values, the displacement parameters of the Rb and K sites, respectively, were unreasonably small (U_{iso} < 0.002 Å^2). (3) As the anisotropic refinement using mixed Cs/M sites always yielded only slightly larger R values but very reasonable displacement parameters, these results were chosen as the best refinements of these solid solutions.

However, it should be noted that the different treatments only resulted in different structural R values and did not affect the profile fit significantly. The occupation factors for all refinements also differed by a maximum of only 2 %. Table 1 lists the crystallographic data of all refined $Cs_{1-x}M_xGaQ_2$-*mC*16 (M = K, Rb; Q = S, Se) phases. The atom coordinates and displacement parameters are listed in the supplementary material (Tables S1-S10).

Table 1. Crystallographic data of the solid solutions $Cs_{1-x}M_xGaQ_2$-*mC*16 (M = K, Rb; Q = S, Se).

	$Cs_{0.90}K_{0.10}GaS_2$	$Cs_{0.84}Rb_{0.16}GaS_2$	$Cs_{0.76}Rb_{0.24}GaS_2$	$Cs_{0.91}Rb_{0.09}GaSe_2$	$Cs_{0.79}Rb_{0.21}GaSe_2$
M /g·mol^{-1}	257.38	259.17	254.43	356.28	350.59
Space group	Monoclinic, *C*2/*c* (No. 15)				
a /Å	7.431(2)	7.426(1)	7.427(1)	7.653(1)	7.655(1)

Preprints (www.preprints.org) | NOT PEER-REVIEWED | Posted: 20 October 2017 doi:10.20944/preprints201710.0140.v1

Peer-reviewed version available at Crystals 2017, 7, 379; doi:10.3390/cryst7120379

b /Å	12.171(3)	12.151(2)	12.041(3)	12.482(3)	12.415(2)
c /Å	5.906(1)	5.907(1)	5.908(1)	6.166(1)	6.161(1)
β /°	113.15(2)	113.11(1)	113.24(1)	113.75(2)	113.88(1)
V /Å^3	491.2(2)	490.3(1)	485.5(2)	539.1(2)	535.4(1)
Diffractometer	DESY P02.1 beamline; λ = 0.20717 Å; T = 20 °C				
2θ range; increment	0.7° < 2θ < 15°; $\Delta\theta$ = 0.004°				
Structure solution	Charge flipping, SUPERFLIP [12]				
Structure refinement	Full matrix against F^2, Jana2006 [13]				
Background	Manual background combined with 8 – 10 Legendre polynoms				
Reflection profile	Pseudo-Voigt function; Refined parameters GW, GU, LY				
No. of parameters	39	38	39	37	39
μ /mm^{-1}	1.546	1.512	1.407	1.879	1.767
GooF	1.74	1.04	1.26	2.80	2.62
R_p, wR_p	0.0069, 0.0097	0.0045, 0.0061	0.0060, 0.0075	0.0104, 0.0143	0.0093, 0.0131
R_1, wR_2 ($I > 3\sigma(I)$)	0.0173, 0.0244	0.0185, 0.0241	0.0197, 0.0256	0.0284, 0.0412	0.0114, 0.0158
R_1, wR_2 (all data)	0.0173, 0.0244	0.0185, 0.0241	0.0197, 0.0256	0.0284, 0.0412	0.0114, 0.0158

[a] Further details on the crystal structures may be obtained from the Fachinformationszentrum Karlsruhe, 76344 Eggenstein-Leopoldshafen, Germany (fax: (+49)7247-808-666; E-mail: crysdata@fiz-karlsruhe.de), on quoting the depository numbers CSD-XXXXXX…

3. Discussion and Summary

Our investigations on the solid solutions series $Cs_{1-x}M_xGaQ_2$-$mC64$ (M = K, Rb; Q = S, Se; x = 0 - 1) revealed, that the formation of such solid solutions is indeed possible. Depending on the chalcogenide and alkali metal combination, however, different mixing behavior is observed. In general, the sulfide mixtures reveal a miscibility gap, while the selenides form complete solid solution series for both, K and Rb. While the possibility of such a gap is only hinted at by the Raman measurements in case of $Cs_{1-x}Rb_xGaS_2$-$mC64$, a decreasing miscibility gap for $Cs_{1-x}K_xGaS_2$-$mC64$ with increasing temperature could be observed in the *in situ* X-ray experiments.

Upon heating of cesium-rich solid solutions, a phase transition similar to the pure cesium phases, *i.e.* a transformation of the 2D anionic network to 1D strands,[6-7] takes place. This process was investigated *in situ* using X-ray powder diffraction techniques. Up to a degree of substitution of approximately 60 at% a phase transition could be detected. An in depth analysis, however, revealed, that phase pure samples of the high-temperature polymorphs could only be obtained up to 30 at% substitution of cesium. A degree of substitution of 0.3 < x < 0.6 leads to a phase separation into a mixture of a cesium rich solid solution $Cs_{1-x}M_xGaQ_2$-$mC16$ and a corresponding rubidium/potassium rich phase $Cs_{1-x}M_xGaQ_2$-$mC64$ where the phase transition is suppressed. Substituting more than 60 at% of cesium completely suppresses the phase transition. The crystal structures of several high-temperature polymorphs $Cs_{1-x}M_xGaQ_2$-$mC16$ (M = K, Rb; Q = S, Se) were refined from synchrotron powder diffraction data by Rietveld refinement. The combination of all these results leads to the quasi-binary phase diagrams $CsGaQ_2$ – $MGaQ_2$, which are depicted in Figure 5.

Preprints (www.preprints.org) | NOT PEER-REVIEWED | Posted: 20 October 2017 doi:10.20944/preprints201710.0140.v1

Peer-reviewed version available at Crystals 2017, 7, 379; doi:10.3390/cryst7120379

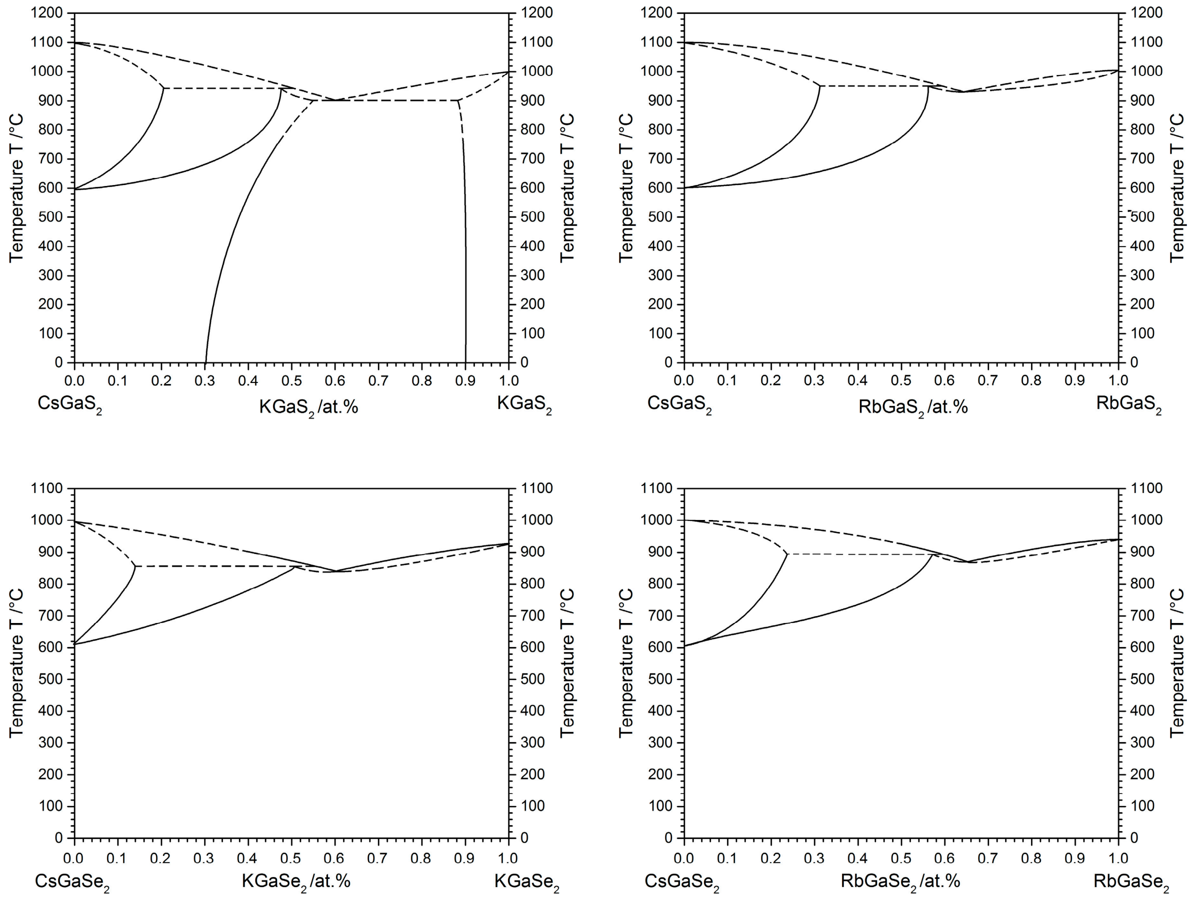

Figure 5. Schematic quasi-binary phase diagrams of the solid solutions $Cs_{1-x}K_xGaS_2$-*mC*64, $Cs_{1-x}Rb_xGaS_2$-*mC*64, $Cs_{1-x}K_xGaSe_2$-*mC*64, and $Cs_{1-x}Rb_xGaSe_2$-*mC*64. The solid lines are based on actual measurements, while the dashed lines represent physically plausible interpolations based on our observations.

Analysis of the solid solutions using UV/Vis and Raman spectroscopy revealed further details on the bonding situation in these and related chalcogenometallates. Prior investigations using DFT calculations reported in [6-8] already revealed covalent Ga-*Q* (*Q* = S, Se) interactions in these kind of substances, which is in accordance with chemical expectation. The character of the alkali metals is mainly ionic, which is concluded from the unoccupied K-4*s*, Rb-5*s* und Cs-6*s* states. These findings are further confirmed by the Raman spectra of all solid solutions. The pattern of valence and deformation vibrations is more or less identical for all sulfides and selenides, respectively, regardless of the nature of the alkali metals. Only the Ga-*Q* vibrations of the extended anions are observed by vibrational spectroscopy (lattice vibrations are of course excluded). Substitution of the alkali metals only leads to a slight blue shift of the Raman bands due to the different ionicity of the alkali metals and the shorter distances *d*(Ga-*Q*) in the rubidium and potassium compounds. Another consequence of the ionic bonding character of the alkali metals can be derived from the optical bandgaps. As the highest occupied alkali metal states (K-3*p*, Rb-4*p* or Cs-5*p*) are located at energies below -10 eV, the states near the band gap are dominated by the Ga-4*s*, Ga-4*p* and the respective *p* states of the chalcogen (S-3*p* or Se-4*p*). The alkali metals, therefore do not significantly contribute to the optical band gaps of these chalcogenometallates as concluded from the almost identical band gaps for all sulfides and selenides, respectively.

Preprints (www.preprints.org) | NOT PEER-REVIEWED | Posted: 20 October 2017 doi:10.20944/preprints201710.0140.v1

Peer-reviewed version available at *Crystals* **2017**, *7*, 379; doi:10.3390/cryst7120379

4. Materials and Methods

4.1 Synthesis of the starting materials

Pure KN_3, RbN_3 and CsN_3 were obtained by passing hydrazoic acid (prepared by acidifying an aqueous solution of NaN_3 (Sigma-Aldrich 99.0%)) into an aqueous solution of K_2CO_3 (Sigma-Aldrich 99 %), Rb_2CO_3 (Sigma-Aldrich 99 %) or Cs_2CO_3 (Rockwood Lithium 99.9 %), respectively. **Attention:** Condensed NH_3 is highly explosive; therefore tools made from transition metals must be avoided. The binary gallium starting materials Ga_2S_3 and GaSe were prepared by annealing stoichiometric mixtures of Ga (Chempur 99.999 %) and the corresponding chalcogen (Chempur 99.999 %) at 1000 °C (Ga_2S_3) and 850 °C (GaSe), respectively.

4.2. Synthesis of KGaQ₂, RbGaQ₂ and CsGaQ₂-mC64 (Q = S, Se)

The ternary compounds were obtained by slow, controlled thermal decomposition of the respective alkali metal azide, combined with a stoichiometric mixture of the binary starting materials and elemental chalcogens in a quartz ampoule under dynamic vacuum conditions (0.3 g batch size, heating rate 0.5 °C/min). After complete decomposition of the azides, the resulting raw products were annealed in flame sealed ampoules at 800 °C (for $KGaQ_2$ and $RbGaQ_2$) and 550 °C (for $CsGaQ_2$-*mC*64), respectively.

4.3. X-ray powder diffraction

The X-ray powder diffraction measurements were carried out on a STOE STADI P diffractometer equipped with a Dectris Mythen 1K detector and a STOE high-temperature capillary furnace. Monochromatic Cu-$K\alpha_1$ radiation (λ = 1.540598 Å) was used for the ambient temperature measurements, while Mo-$K\alpha_1$ radiation (λ = 0.709300 Å) was used for the non-ambient experiments. For the high-temperature measurements, powdered samples were loaded in quartz capillaries (diameter 0.3 mm) and investigated in the temperature region from 25 – 900 °C in steps of 10 °C (4.55° < 2θ < 23.42°, irradiation time 5 min per diffraction pattern). The furnace temperature was controlled by a Eurotherm 24.16 controller (ΔT = ±1 °C). The samples were held at the respective temperature for 3 min prior to each measurement to ensure thermal equilibrium. The WinX^{POW} software package from STOE & Cie was used for data collection and processing [16].

4.4. Rietveld refinement

The X-ray powder diffraction patterns for the Rietveld refinements were collected at the beamlineP02.1 at Petra III (DESY, Hamburg). A monochromatic photon energy of approximately 60 keV corresponding to a wavelength of λ = 0.20717 Å and a beam size of 0.7 x 0.7 mm was used for all experiments. For the data acquisition, a PerkinElmer XRD1621 fast area detector and a sample to detector distance of 710 mm was used. The 2D data was integrated using the FIT2D software [17]. Powdered samples were measured in quartz glass capillaries (diameter 0.7 mm) with an irradiation time of 90 s for all experiments. The Rietveld refinement was performed using Jana2006 [15]. A manual background combined with 8-10 Legendre polynoms was used for all diffraction patterns. The peak profiles were described by Pseudo Voigt functions refining the parameters GW, GU and LY. The occupation factors of the mixed alkali metal sites were refined using a restraint in order to ensure charge balance. All other positions were fully occupied. The atomic coordinates and anisotropic displacement parameters were refined without any restraints.

4.5. Raman spectroscopy

The Raman spectra were recorded on a DXR™ SmartRaman Spectrometer from Thermoscientific (excitation wavelength λ = 532 nm) in the range of 50-1000 cm^{-1} with a resolution of 0.5 cm^{-1}.

4.6. UV/Vis Diffuse reflectance spectroscopy

Diffuse reflectance spectra were measured with a Bruins Omega 20 UV/Vis spectrometer using $BaSO_4$ as a white standard (100% reflectance). The absorption data was calculated using a modified Kubelka-Munk function [18].

Supplementary Materials: The following data are available online at www.mdpi.com/link, Figure S1: X-ray diffraction patterns of the solid solution series $Cs_{1-x}K_xGaS_2$-*mC*64, Figure S2: X-ray diffraction patterns of the solid solution series $Cs_{1-x}Rb_xGaS_2$-*mC*64, Figure S3: X-ray diffraction patterns of the solid solution series $Cs_{1-x}K_xGaSe_2$-*mC*64, Figure S4: X-ray diffraction patterns of the solid solution series $Cs_{1-x}Rb_xGaSe_2$-*mC*64, Figure S5: Evolution of the X-ray powder diffraction patterns of all solid solutions in the temperature region from 20 – 900 °C, Figure S6 Plot of the Rietveld refinement of the X-ray diffraction pattern of $Cs_{0.90}K_{0.10}GaS_2$-*mC*16, Table S1 Atomic coordinates and isotropic displacement parameters for $Cs_{0.90}K_{0.10}GaS_2$-*mC*16, Table S2 Anisotropic displacement parameters for $Cs_{0.90}K_{0.10}GaS_2$-*mC*16, Figure S7 Plot of the Rietveld refinement of the X-ray diffraction pattern of $Cs_{0.84}Rb_{0.16}GaS_2$-*mC*16, Table S3 Atomic coordinates and isotropic displacement parameters for $Cs_{0.84}Rb_{0.16}GaS_2$-*mC*16, Table S4 Anisotropic displacement parameters for $Cs_{0.84}Rb_{0.16}GaS_2$-*mC*16,Figure S8 Plot of the Rietveld refinement of the X-ray diffraction pattern of $Cs_{0.74}Rb_{0.26}GaS_2$-*mC*16, Table S5 Atomic coordinates and isotropic displacement parameters for $Cs_{0.74}Rb_{0.26}GaS_2$-*mC*16, Table S6 Anisotropic displacement parameters for $Cs_{0.74}Rb_{0.26}GaS_2$-*mC*16, Figure S9 Plot of the Rietveld refinement of the X-ray diffraction pattern of $Cs_{0.91}Rb_{0.09}GaSe_2$-*mC*16, Table S7 Atomic coordinates and isotropic displacement parameters for $Cs_{0.91}Rb_{0.09}GaS_2$-*mC*16, Table S8 Anisotropic displacement parameters for $Cs_{0.91}Rb_{0.09}GaS_2$-*mC*16, Figure S10 Plot of the Rietveld refinement of the X-ray diffraction pattern of $Cs_{0.79}Rb_{0.21}GaSe_2$-*mC*16, Table S9 Atomic coordinates and isotropic displacement parameters for $Cs_{0.79}Rb_{0.21}GaSe_2$-*mC*16, Table S10 Anisotropic displacement parameters for $Cs_{0.79}Rb_{0.21}GaSe_2$-*mC*16.

Acknowledgments: *The authors would like to thank Dr. Václav Petříček (Czech Academy of Sciences, Prague) for his helpful comments regarding the handling of the mixed occupations during the Rietveld refinement. We would further like to thank Prof. Dr. Manfred Scheer (University of Regensburg) for the Raman measurements, Tamara Woppmann for reproducing the rubidium solid solutions in the course of her bachelor thesis, and Rockwood-Lithium for supplying cesium carbonate.*

References

1. V. Petrov, A. Yelisseyev, L. Isaenko, S. Lobanov, A. Titov, J. J. Zondy, "Second harmonic generation and optical parametric amplification in the mid-IR with orthorhombic biaxial crystals $LiGaS_2$ and $LiGaSe_2$" *Appl. Phys. B: Laser Opt.* **2004**, *78*, 543-546, 10.1007/s00340-004-1463-0.
2. B. Krebs, "Thio- und Selenoverbindungen von Hauptgruppenelementen - neue anorganische Oligomere und Polymere" *Angew. Chem.* **1983**, *95*, 113-134, 10.1002/ange.19830950206.
3. D. Müller, F. E. Poltmann, H. Hahn, "Zur Struktur ternärer Chalkogenide des Thalliums mit Aluminium, Gallium und Indium. XXII" *Z. Naturforsch.* **1974**, *29B*, 117-118, 10.1515/znb-1974-1-237.
4. J. A. A. Ketelaar, W. H. t'Hart, M. Moerel, D. Polder, " The Crystal Structure of TlSe, Thallous Thallic or Thallosic Selenide" *Z. Kristallogr. – Cryst. Mater* **1939**, 101, 396-405, 10.1524/zkri.1939.101.1.396.
5. J. W. Boon, C. H. Mac Gillavry, "The crystal structure of potassium thioferrite $KFeS_2$ and sodium thiochromite $NaCrS_2$" *Rec. Trav. Chem. Pays-Bas* **1942**, *61*, 910-920, 10.1002/recl.19420611214.
6. D. Friedrich, M. Schlosser, R. Weihrich, A. Pfitzner, "Polymorphism of $CsGaS_2$ - structural characterization of a new two-dimensional polymorph and study of the phase-transition kinetics" *Inorg. Chem. Front.* **2017**, *4*, 393-400, 10.1039/C6QI00462H.
7. D. Friedrich, M. Schlosser, A. Pfitzner, "Synthesis, Crystal Structure, and Physical Properties of Two Polymorphs of $CsGaSe_2$, and High-Temperature X-ray Diffraction Study of the Phase Transition Kinetics" *Cryst. Growth. Des.* **2016**, *16*, 3983-3992, 10.1021/acs.cgd.6b00532.
8. K. Feng, D. Mei, L. Bai, Z. Lin, J. Yao, Y. Wu, "Synthesis, structure, physical properties, and electronic structure of $KGaSe_2$" *Solid State Sciences* **2012**, *14*, 1152-1156, 10.1016/j.solidstatesciences.2012.05.028.
9. P. Lemoine, D. Carre, M. Guittard, "Structure du sulfure de gallium et de potassium, $KGaS_2$" *Acta Cryst. C* **1984**, *40*, 910-912, 10.1107/S0108270184006223.
10. A. Kumari, K. Vidyasagar, "Rubidium thiogallate" *Acta Cryst. E* **2005**, *61*, i193-i195, 10.1107/S1600536805024815.

 doi:10.20944/preprints201710.0140.v1

Peer-reviewed version available at *Crystals* **2017**, *7*, 379; doi:10.3390/cryst7120379

11. D. Friedrich, M. Schlosser, A. Pfitzner, “Synthesis and Structural Characterization of the Layered Selenogallate $RbGaSe_2$” *Z. Anorg. Allg. Chem.* **2017**, in press.
12. E. J. Wu, M. A. Pell, T. M. Fuelberth, J. A. Ibers, "Crystal structure of cesium gallium ditelluride, $CsGaTe_2$" *Z. Kristallogr. – New Cryst. Struct.* **1997**, 212, 91, 10.1524/ncrs.1997.212.1.91.
13. D. Friedrich, M. Schlosser, A. Pfitzner, “Interconversion of One-Dimensional Thiogallates $Cs_2[Ga_2(S_2)_{2-x}S_{2+x}]$ ($x = 0, 1, 2$) by Using High-Temperature Decomposition and Polysulfide-Flux Reactions” *Cryst. Growth Des.*, **2017**, 17(9), 4887–4892, 10.1021/acs.cgd.7b00840.
14. L. Palatinus, G. Chapuis, "SUPERFLIP - a computer program for the solution of crystal structures by charge flipping in arbitrary dimensions" *J. Appl. Cryst.* **2007**, *40*, 786-790, 10.1107/S0021889807029238.
15. V. Petříček, M. Dušek, L. Palatinus, "Crystallographic Computing System JANA2006: General features" *Z. Kristallogr. – Cryst. Mater.* **2014**, *229*, 345, 10.1515/zkri-2014-1737.
16. STOE WinX^{POW}, Version 3.10, STOE & Cie GmbH, Darmstadt, **2017**,
17. A. P. Hammersley, S. O. Svensson, M. Hanfland, A. N. Fitch, D. Hausermann, "Two-dimensional detector software: From real detector to idealised image or two-theta scan" *High Press. Res.* **1996**, *14*, 235-248, 10.1080/08957959608201408.
18. H. Kisch, "Semiconductor Photocatalysis—Mechanistic and Synthetic Aspects" *Angew. Chem. Int. Ed.* **2013**, *52*, 812-847, 10.1002/anie.201201200.